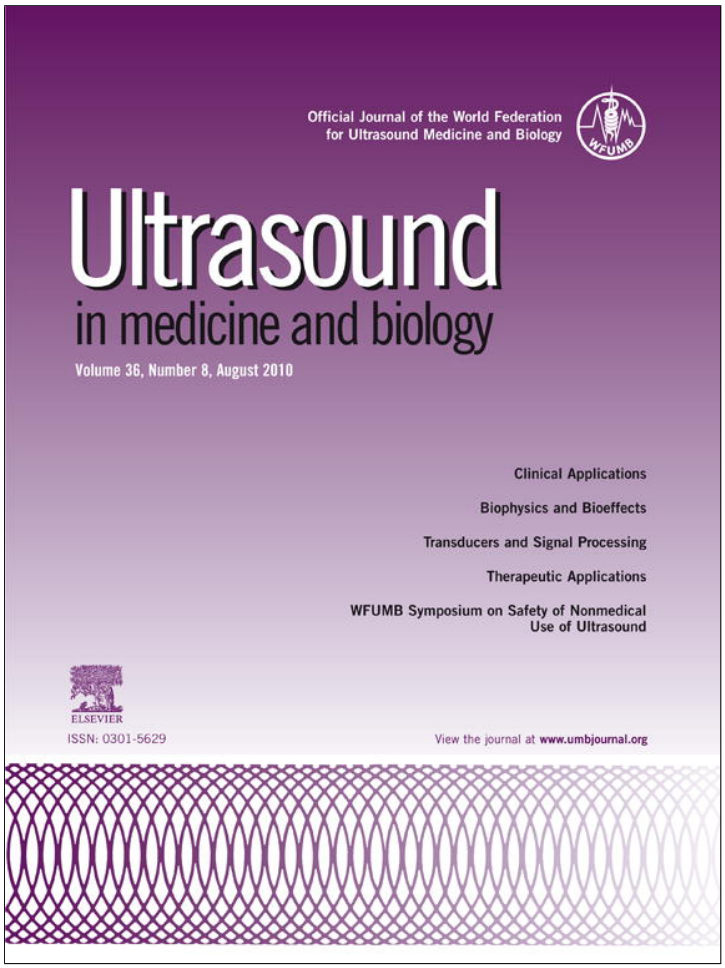

Ultrasound in Med. & Biol., Vol. 36, No. 8, pp. 1245–1258, 2010

0301-5629/$ - see front matter

ELSEVIER

doi:10.1016/j.ultrasmedbio.2010.05.009

● *Original Contribution*

A NEW APPROACH FOR IMPROVING CORONARY PLAQUE COMPONENT ANALYSIS BASED ON INTRAVASCULAR ULTRASOUND IMAGES

Arash Taki,* Holger Hetterich,† Alireza Roodaki,‡ S. K. Setarehdan,§ Gozde Unal,¶ Johannes Rieber,† Nassir Navab,* and Andreas König†

*Department of Computer Aided Medical Procedures (CAMP), Technical University of Munich (TUM), Munich, Germany; †Department of Cardiology, Klinikum der Universitat Munchen, Medizinische Poliklinik-Campus, Innenstadt, Munich, Germany; ‡Department of Signal Processing and Electronic Systems, Supelec, Gif-sur-Yvette, France; §Control and Intelligent Processing Center of Excellence, School of Electrical and Computer Engineering, College of Engineering, University of Tehran, Tehran, Iran; and ¶Faculty of Engineering and Natural Sciences, Sabanci University, Turkey

(*Received* 12 *October* 2009; *revised* 26 *April* 2010; *in final form* 8 *May* 2010)

Abstract—Virtual histology intravascular ultrasound (VH-IVUS) is a clinically available technique for atherosclerosis plaque characterization. It, however, suffers from a poor longitudinal resolution due to electrocardiogram (ECG)-gated acquisition. This article presents an effective algorithm for IVUS image-based histology to overcome this limitation. After plaque area extraction within an input IVUS image, a textural analysis procedure consisting of feature extraction and classification steps is proposed. The pixels of the extracted plaque area excluding the shadow region were classified into one of the three plaque components of fibro-fatty (FF), calcification (CA) or necrotic core (NC) tissues. The average classification accuracy for pixel and region based validations is 75% and 87% respectively. Sensitivities (specificities) were 79% (85%) for CA, 81% (90%) for FF and 52% (82%) for NC. The kappa (κ) = 0.61 and p value = 0.02 indicate good agreement of the proposed method with VH images. Finally, the enhancement in the longitudinal resolution was evaluated by reconstructing the IVUS images between the two sequential IVUS-VH images. (E-mail: taki@cs.tum.edu) **© 2010 World Federation for Ultrasound in Medicine & Biology.**

Key Words: **IVUS, Plaque component analysis, Shadow region, Longitudinal resolution, Virtual histology.**

INTRODUCTION

Gray-scale intravascular ultrasound (IVUS) enables real-time and high-resolution tomographic visualization of the coronary arteries. Both lumen and vessel dimensions and the distribution of plaques can be analyzed by IVUS data. Additionally, plaque rupture and intraluminal thrombus presence might be detected by gray-scale IVUS (Virmani et al. 2003). Each plaque component, consisting of fibrous, calcification, necrotic core and lipid reflect the radio-frequency (RF) signal back in a different way. This affects the resulting IVUS image in a way that an expert might be able to distinguish the different echogenicity of the plaque component.

This, however, is not a simple task even for an expert to characterize an IVUS image. Soft plaques, which are mostly related to lipid, are known by dark intensities. On the other hand, hard plaques consisting of fibrous and calcium components generate intermediate to high intensities. Limitations of IVUS in the plaque characterization arise from the fact that the observable characteristics and relations among atherosclerotic plaque constituents and their presentation in a cross-sectional IVUS image do not follow a simple pattern. For instance, fibrous plaques usually have an intermediate intensity but sometimes very dense fibrous plaques can also resemble calcified regions (Böse et al. 2007; Gonzalo et al. 2008; Mintz et al. 2001) or while acoustic shadowing has been considered as a calcification characteristic, necrotic tissue can also cause shadowing (Bruining et al. 2007; Gonzalo et al. 2008). Moreover, manual analysis of the cross- sectional images is both time consuming and prone to interobserver and intraobserver variability. These limitations in the manual IVUS plaque assessment have led to development of automatic quantitative techniques for analyzing plaque components. In general, the procedures of analyzing gray-scale IVUS images can be divided into two aspects: (1) detecting the vessel

Address correspondence to: Arash Taki, TU MÜnchen Institut fr Informatik/I-16, Boltzmannstr. 3 85748 Garching b. Munchen, Germany. E-mail: taki@cs.tum.edu

borders and (2) characterizing the atherosclerosis plaque composition.

The lumen-intima and the media adventitia borders detection can be carried out by using an appropriate segmentation algorithm such as the parametric or the geometric deformable models (Taki et al. 2008) and/or the shape driven methods (Unal et al. 2008). In addition, several techniques have been developed for plaque characterization such as virtual histology (VH) (Nair et al. 2002, 2007), which is clinically available for *in vivo* plaque assessment. VH, which is carried out by ultrasound RF data analysis of the backscattered ultrasound signal, is able to differentiate four plaque components of fibrous, fibro-lipidic, calcified and necrotic tissues with a high sensitivity and specificity (Nair et al. 2002). However, one of the limitations of VH relates to its electrocardiogram (ECG)-gated acquisition. Indeed, owing to RF attenuation and shifting due to the presence of blood in coronary arteries and the high amount of data, VH algorithm resorts to use an ECG-gating procedure. Using the ECG-gated acquisition, in one cardiac cycle, the RF spectrum from only one IVUS frame which is synchronized with the R-wave is acquired and analyzed while gray-scale IVUS images are produced at a rate of 30 frames/s (O'Malley et al. 2007). Therefore, comparing to the rate of the gray-scale IVUS images, the longitudinal resolution for VH is reduced to one image out of 30 frames/s (Fig. 1).

In addition to the ECG-gated acquisition limitation of VH, there are other limitations such as imprecisions in plaque composition analysis caused by the inaccurate border detection used in VH methodology (Frutkin et al. 2007) or the inability of this method in identifying vulnerable and thin cap fibro-atheroma (TCFA) plaque type (Sangiorgi et al. 2007; Sawada et al. 2008). The former is especially important when studying thrombus-laden arteries where inaccurate detection of the borders might introduce large measurement errors of plaque composition. In this case, the proportionality of fibrous plaque may misleadingly increase since the thrombus regions can be labeled as fibrous (Frutkin et al. 2007).

There are also other signal based atherosclerosis plaque characterization methods such as the integrated backscatter IVUS (IB-IVUS) (Okubo et al. 2008; Kawasaki et al. 2005). IB-IVUS can classify plaque components in the IVUS images into five categories of calcification: (1) mixed lesion, (2) fibrous tissue, (3) lipid core or (4) intimal hyperplasia and (5) thrombus, by introducing various thresholds on the IB values (Okubo et al. 2008; Kawasaki et al. 2005). This promising method, currently implemented in a Japanese system (YD Co. Ltd., Tokyo. Japan), uses the IVUS catheter from Boston Scientific (Fremont, CA, USA) based on a 40 MHz single rotating crystal. Although, the IB-IVUS is reported to be more accurate than IVUS-VH in (Okubo et al. 2008) for IB-IVUS, it is not clinically as popular as IVUS-VH. Katouzian et al. (2008a) studied the challenges in atherosclerotic plaque characterization with IVUS backscatters (from data collection to classification) and they developed a texture-based algorithm for plaque characterization in (Katouzian et al. 2008a). They believed that their method

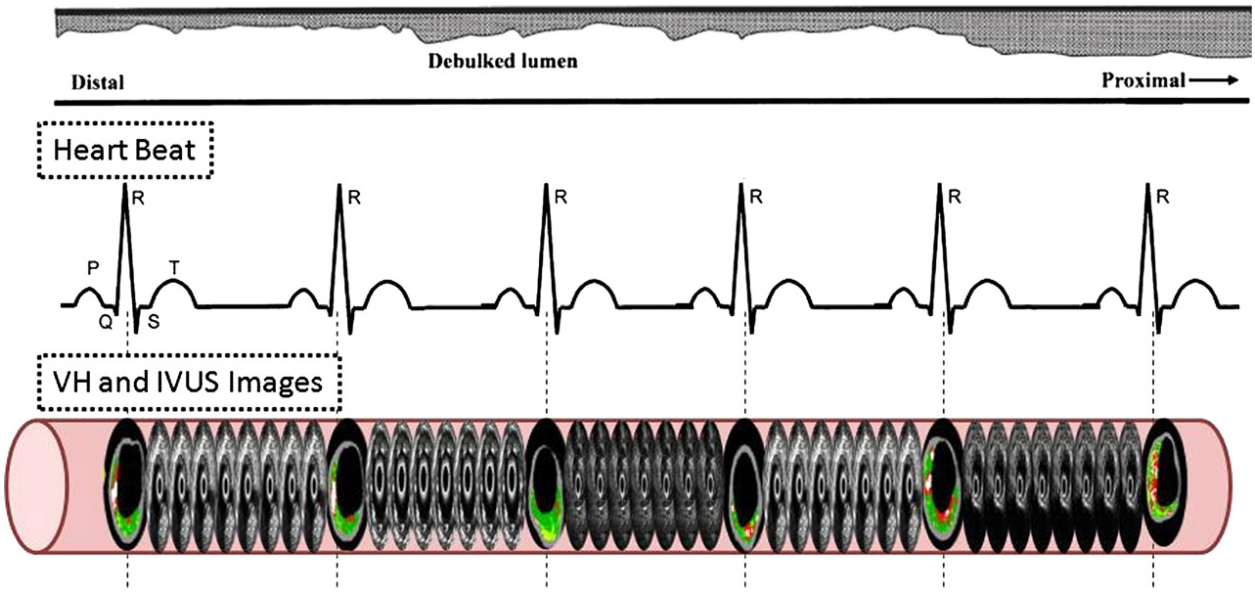

Fig. 1. Illustration of the longitudinal resolution of gray-scale intravascular ultrasound (IVUS) and virtual histology (VH). Gray-scale IVUS images are produced at a rate of 30 frames/s. Considering a heart rate of 60 beats/min and pullback speed of 1 mm/s, radio-frequency (RF) analysis is performed for only one frame/mm (1 frame/s). Therefore, VH has a much lower longitudinal resolution than gray-scale IVUS.

would also resolve one of the main current limitations of IVUS, which is the discrimination between fibrotic and lipidic tissues. All these methods, however, suffer from the ECG-gated acquisition. Since valuable data in the ECG-gated acquisition procedure would be lost, developing an image based characterization technique for complementing the signal- based approach in VH might be of great value. Moreover, by offering an automatic characterization for gray-scale IVUS images between two VH frames, one would be able to increase the longitudinal resolution for plaque composition analysis.

In this article, a new technique is proposed to provide a color-coded characterization of the atherosclerotic plaque component derived from gray-scale IVUS images. Clinically used VH images are considered as validation of the proposed algorithms.

METHODS

The block diagram of the proposed IVUS image based histology (IBH) algorithm is demonstrated in Figure 2. The IVUS images are first transformed into polar coordinates. Then, the automatic border detection method proposed in (Unal et al. 2008) is applied to identify the vessel lumen and media-adventitial borders. The region between the two boundaries is extracted as the *plaque area*. Some IVUS images contain calcified regions causing lateral shadowing; it might be erroneous to classify the plaques contained in the shadow region. Therefore, in the proposed algorithm, the shadow region is detected by means of a thresholding procedure and classified as unknown region called *shadow region*. Next, with the use of a textural analysis technique, the pixels of the defined plaque area excluding the shadow region are classified into one of the three plaque components: fibro-fatty (FF), calcification (CA) or necrotic core (NC) tissues. We choose to combine the fibrous and fibro-fatty tissue classes, since their distinction is of minor clinical importance and technically challenging, using only the information from gray-scale IVUS (Hiro et al. 1997). The overlap between the histogram of these two plaque regions in our data set is highlighted in Figure 3. Finally, by applying a postprocessing technique based on the histogram analysis of the entire data set, the decision of the classifier is corrected.

Image acquisition and RF data analysis

In this work, both IVUS gray-scale and corresponding VH images were acquired from patients with known coronary artery disease. The evaluation of our algorithm is performed over a data set that includes 500 gray-scale IVUS examination performed on 10 patients with known or suspected coronary artery disease during cardiac catheterization resulting in a total number of 12 vessels. Written informed consent was obtained from each patient and the present study was approved by the local

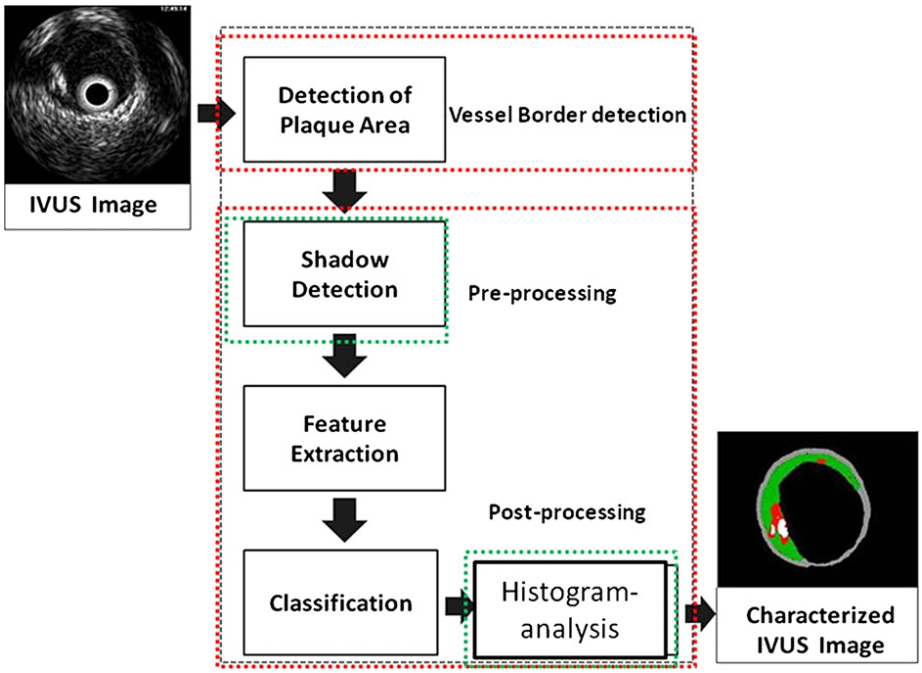

Fig. 2. Scheme of the work flow in the image based histology (IBH) system. First, an IVUS image is loaded. Then, the vessel's borders are detected using automatic border detection. Next, the textural features are extracted from the plaque area and then, support vector machine (SVM) classifier is applied to classify the pixels of the plaque area to generate the color-coded image representing the different plaque components.

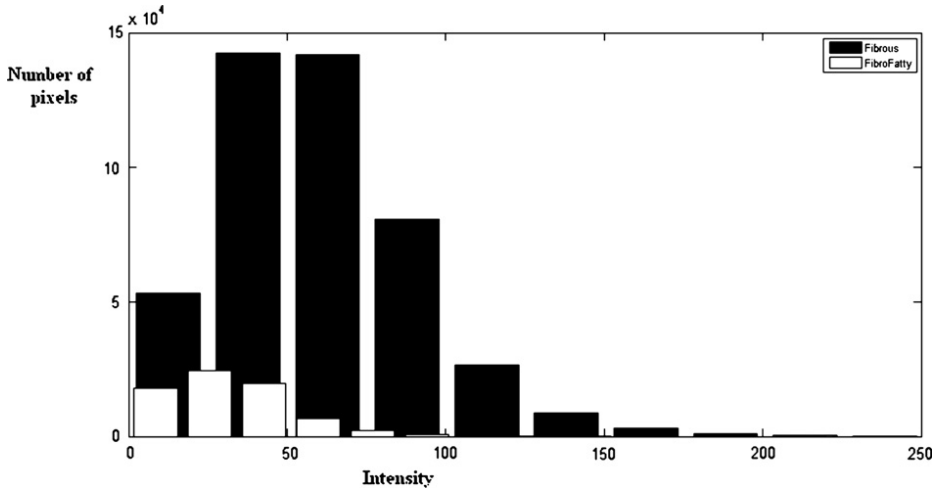

Fig. 3. Histogram of fibro-fatty (white color) and fibrous (black color) plaques extracted from virtual histology (VH) images. The histogram of fibro-fatty class is completely covered by the histogram of the fibrous class.

medical ethics committee. The catheter and guidewire were introduced over the femoral approach using standard techniques and the right or left coronary artery ostium was cannulated. After placement of the guidewire, the IVUS imaging catheter (Eagle Eye Gold, Volcano Inc., Rancho Cordova, CA, USA) was introduced and placed at the distal part of the artery under fluoroscopic guidance.

The main features of the Eagle Eye Gold catheter are as follows: frequency, 20 MHz, scanner diameter, 3.5F, compatible with 0.014-inch guidewire and field of view, 16 mm. With the help of a s5i-system (Volcano Inc., Rancho Cordova, CA, USA), data for gray-scale IVUS and RF analysis was acquired, during automatic pullback at a speed of 0.5 mm/s using a dedicated pullback device (Track Back II; Volcano Inc., Rancho Cordova, CA, USA) up to the ostium of the coronary. For offline analysis, the data was stored on a DVD. The RF data was analyzed with the VH image analysis software (Volcano Inc.) after automatic border detection and manual correction of the borders. The corresponding gray-scale IVUS frames were stored in the JPG-format for further analysis.

Plaque area detection

The inner and outer walls of the coronary arteries were extracted from each IVUS image before the plaque characterization. We utilized the method presented by Unal et al. (Unal et al. 2008) for segmentation of the lumen and media-adventitia borders of the coronary arteries that have been extensively described elsewhere (Unal et al. 2008). Briefly, this approach entails representing the luminal and media-adventitial borders in the polar image with a reduced number of contour weights, which are obtained from a constructed statistical shape space. The two arterial wall borders presented by this segmentation method (*i.e.* the lumen and media-adventitia contours) are passed as plaque area to the next stage for plaque characterization.

Plaque characterization

The main purpose of the current research is to propose a plaque characterization method consisting of feature extraction and classification steps. Each pixel of the IVUS image will be assigned to one of the three predefined tissue classes. Note that in this section, for a matching comparison and validation of our characterization algorithm, against ECG-triggered VH-IVUS cross-sectional areas, the detected plaque area in VH images surrounded by gray colored region is directly used. An important fact, which is ignored in characterizing atherosclerosis plaques via features extracted from IVUS images, is to detect the acoustic shadowing behind CA regions and treat them differently. These shadow regions, which exist in the plaque area of some IVUS image scenarios, appear as echo-soft. Therefore, when treated within other parts of plaque area, they are classified as the lipid or fibro-fatty classes whereas they normally should be classified into CA and NC plaques (Bruining et al. 2007; Mintz et al. 2001).

Shadow detection

Shadow areas displayed in the IVUS gray-scale images usually do not represent any useful information for plaque component analysis. Nevertheless, VH-IVUS extracts information in shadow area from frequency of ultrasound backscatter signals. However, VH-IVUS results may differ in shadow area from the histology interpretations of pathologists with varying interpretive methodologies as shown in Figure 4 (König et al. 2008). By defining a specific plaque region as *shadow region*, we aimed at reducing the above-mentioned errors that are caused by the nature of ultrasound imaging. For detecting

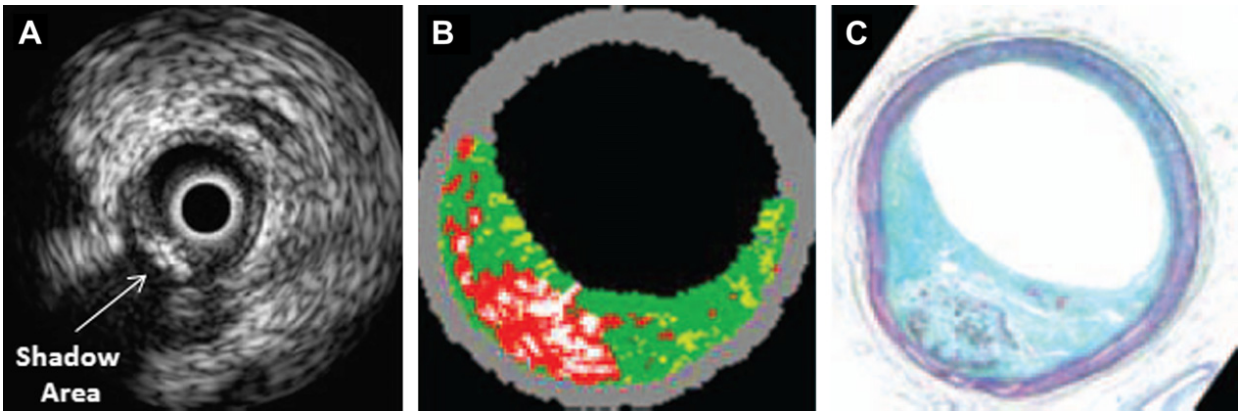

Fig. 4. The shadow region in a typical intravascular ultrasound (IVUS) gray-scale image (A), its plaque constituents in intravascular ultrasound-image based histology (IVUS-IBH) (B) and its corresponding histopathalogy (C) (König et al. 2008).

this region, our proposal is to use a preprocessing step consisting of two thresholding parts; one for detecting the high intensity regions, which might belong to CA and the other is to identify the existence of the low intensity regions behind the regions detected in the previous step and assign them to the *shadow region* (see Fig. 4).

Feature extraction methods

To characterize the rest of plaque area to the three predefined plaque components, two feature extraction methods are examined and compared. To achieve this purpose, local binary pattern (LBP) (Ojala et al. 2002) and co-occurrence (Haralick et al. 1973) feature extraction methods are studied in (Caballero et al., 2006) and are reported to out perform other feature extraction methods. Moreover, it is reported in (Vince et al., 2000) that the run-length method (Tang 1998) is not an appropriate feature extraction method for characterizing IVUS images plaque area. In Escalera et al. (2008), both signal and image-based features are extracted. The co-occurrence, LBP and Gabor filtering feature extraction methods are used for texture-based feature extraction. Their results are compared with manual characterization of IVUS images by two experts and 90% accuracy is achieved. However, the manual characterization of IVUS images suffer from both interobserver and intraobserver variability and especially uncertainty in characterizing soft plaques from each other, *e.g.*, distinguishing between the FF and the NC tissues.

Here, the performance of the features extracted from the run-length matrix is compared with those extracted from the LBP method in both accuracy and time efficiency aspects. The co-occurrence feature extraction method is not included in this study since our previous studies reveal that despite good performance of this method in atherosclerotic plaque characterization, its heavy computational burden leads to poor time efficiency (Taki et al., 2009).

IVUS imaging provides circular cross-section areas of the blood vessel and it uses 256 scan lines, therefore, the lateral resolution is 360/256 = 1.41 degrees and the axial resolution is about 40 microns. Since IVUS images are circular cross-sectional areas of coronary arteries, the plaque area of the input images are converted into polar coordinates so that rectangular sweeping windows used for feature extraction are applicable. Throughout this article, the image refers to the converted image. The polar transformed image is then swept by a sweeping window. The size of the sweeping window for both feature extraction techniques was empirically chosen as 9 × 9 pixels (pixel = 0.025 mm).

Local binary pattern. Local binary pattern (LBP) is a structure-related measure in which a binary number is allocated to the circularly symmetric neighborhoods of the center pixel of the window being processed and the histogram of the resulting binary patterns can be used as a discriminative feature for texture analysis (Caballero et al., 2006; Escalera et al., 2008; Ojala et al., 2002; Vince et al., 2000). Actually, in this method neighbors of the center pixel on a circle of radius R with coordinates $(-R \sin \frac{\pi n}{N}, R \cos \frac{\pi n}{N})(n = 0, \ldots, N-1)$ are processed. As these coordinates do not match the coordinates of the processing window, their corresponding gray levels are estimated by interpolation. Let g_c corresponds to the gray value of the central pixel and g_n corresponds to the gray values of the n neighbor pixels. A binary digit is then allocated to each neighbor based on the following function:

$$s(g_n - g_c) = \begin{cases} 1, & g_n - g_c \geq 0 \\ 0, & g_n - g_c < 0 \end{cases} \quad (1)$$

Then, by rotating the neighbor set clockwise, the least significant resulting binary string is assigned to the processing as its binary pattern $L_{R,N} = \{L^0_{R,N}, \ldots, L^{N-1}_{R,N}\}$. In this way, the local binary pattern is rotation-invariant. Based on the binary pattern $L_{R,N}$ and the gray values of neighbor pixels $g_{n,}$ three texture features are defined as follows:

$$f^1_{R,N} = \sum_{n=0}^{N-1} L^n_{R,N}\, 2^n \tag{2}$$

$$f^2_{R,N} = \mathrm{var}\{g_n\} \tag{3}$$

$$f^3_{R,N} = \begin{cases} \sum_{n=0}^{N-1} L^n_{R,N}, U(L_{R,N}) \le 0 \\ N+1, otherwise \end{cases} \tag{4}$$

Function U is a transition counter that counts the transition between 0 and 1 and vice versa in the binary pattern.

Extended run-length. Run-length transform (Tang 1998) has been extensively used in segmentation and texture analysis. Let us consider the neighborhood *I(v,w)* centered on the pixel *(x,y)* from image *I*. Its run-length matrix is defined in a certain direction as *R(a,b)* where $a \in [1,N_g]$ is the gray level, N_g is the highest gray level and b the run-length, *i.e.*, the number of consecutive pixels along a direction having the same gray level value. In our approach, we characterize each

Table 1. Definition and formulas of features extracted from run-length matrix

Extended run-length features		
Definition	$R_k(a,b): \alpha \in [1,..,P]$ is the gray level and b is the run-length; k determines the direction (v means vertical and h means horizontal) N_r: the total number of runs N_p: the number of pixels in the processing window	
Extracted features	Short run emphasis (SRE)	$f_1^k = \frac{1}{N_r}\sum_{a=1}^{P}\sum_{b=1}^{R}\frac{Rk(a,b)}{b^2}$
	Long run emphasis (LRE)	$f_2^k = \frac{1}{N_r}\sum_{a=1}^{P}\sum_{b=1}^{R} R_k(a,b)\cdot b^2$
	Gray-level nonuniformity (GLN)	$f_3^k = \frac{1}{N_r}\sum_{a=1}^{P}\left(\sum_{b=1}^{R} R_k(a,b)\right)^2$
	Run length nonuniformity (RLN)	$f_4^k = \frac{1}{N_r}\sum_{b=1}^{R}\left(\sum_{a=1}^{P} R_k(a,b)\right)^2$
	Run percentage (RP)	$f_5^k = \frac{N_r}{N_p}$
	Low gray-level run emphasis (LGRE)	$f_6^k = \frac{1}{N_r}\sum_{a=1}^{P}\sum_{b=1}^{R}\frac{Rk(a,b)}{a^2}$
	High gray-level run emphasis (HGRE)	$f_7^k = \frac{1}{N_r}\sum_{a=1}^{P}\sum_{b=1}^{R} R_k(a,b)\cdot a^2$
	Short run low gray-level run emphasis (SRLGE)	$f_8^k = \frac{1}{N_r}\sum_{a=1}^{P}\sum_{b=1}^{R}\frac{R_k(a,b)^2}{a^2\cdot b^2}$
	Short run high gray-level run emphasis (SRHGE)	$f_9^k = \frac{1}{N_r}\sum_{a=1}^{P}\sum_{b=1}^{R}\frac{R_k(a,b)\cdot a^2}{b^2}$
	Long run low gray-level run emphasis (LRLGE)	$f_{10}^k = \frac{1}{N_r}\sum_{a=1}^{P}\sum_{b=1}^{R}\frac{R_k(a,b)\cdot b^2}{a^2}$
	Long run high gray-level run emphasis (LRHGE)	$f_{11}^k = \frac{1}{N_r}\sum_{a=1}^{P}\sum_{b=1}^{R} R_k(a,b)\cdot a^2\cdot b^2$

The first five features are called conventional features here. The whole 11 features are named to be extended run-length features.

neighborhood with two run-length matrices $R_v(a, b)$ and $R_h(a,b)$ corresponding to vertical and horizontal directions, respectively.

Table 1 contains the definitions and formulas used for computing features extracted from the run-length matrix. Here, the first five features, called conventional features, have been previously used on IVUS images although the results were not satisfactory (Vince et al., 2000). In fact, these features are not appropriate for describing texture gray-level information and they just consider the length of runs. However in (Tang 1998), other textural information are extracted from the run-length matrix. Since most of the discriminative information lies in the homogeneity of specific intensities in different plaque components, run-length matrix might be a good choice for feature extraction part. Adding the six features, shown as f_6 to f_{11} in Table 1, to the five conventional ones enable us to encode the desired information of run-length matrix. These 11 features are called the extended run-length features.

Support vector machine classifier

In this study, the extracted features from the plaque area of IVUS images are classified using support vector machine (SVM) classifier. SVMs (Burges 1998; Chang and Lin 2001) use a kernel function to map the input to a higher dimensional space where a hyper-plane can separate the data into different classes. The process of training an SVM classifier is equivalent to finding this optimal hyper-plane by minimizing their misclassification error. We consider the worst case of nonseparable tissue classes and use the Gaussian radial basis function (RBF) kernel to handle nonlinear relations between feature vectors and their classes with few parameters. For more detailed information, please refer to the article by Burges (1998). All extracted feature vectors were normalized into [0, 1] before applying the classifier. The Gaussian kernel with the standard deviation of 0.7 was employed in the SVM classifier. We used the publicly available C++ implementation of the SVM algorithms known as LIBSVM (Chang and Lin 2001).

Postprocessing

Studying intensity variety of each plaque component in VH images of our data set through histogram analysis reveals that useful information can be extracted via this simple analysis. Figure 5 illustrates the histogram of pixels for three different plaque components. As this gray-scale derived information might be ignored amongst the many textural features in the classification steps, another step is added to the algorithm after the classification is completed by SVM. In this step, the given label of a pixel by SVM is confirmed or altered based on some prior information derived from the histogram of the IVUS image. Some useful information is pointed out below that can be inferred from the histograms displayed in Figure 5.

- The majority of samples belong to the FF class; however, there are few FF pixels whose intensities exceed the gray-level 150 ($ThFF = 150$).
- Most of the pixels with intensities above the gray-level 200 ($ThCA(\text{low}) = 200$) belong to the CA class,

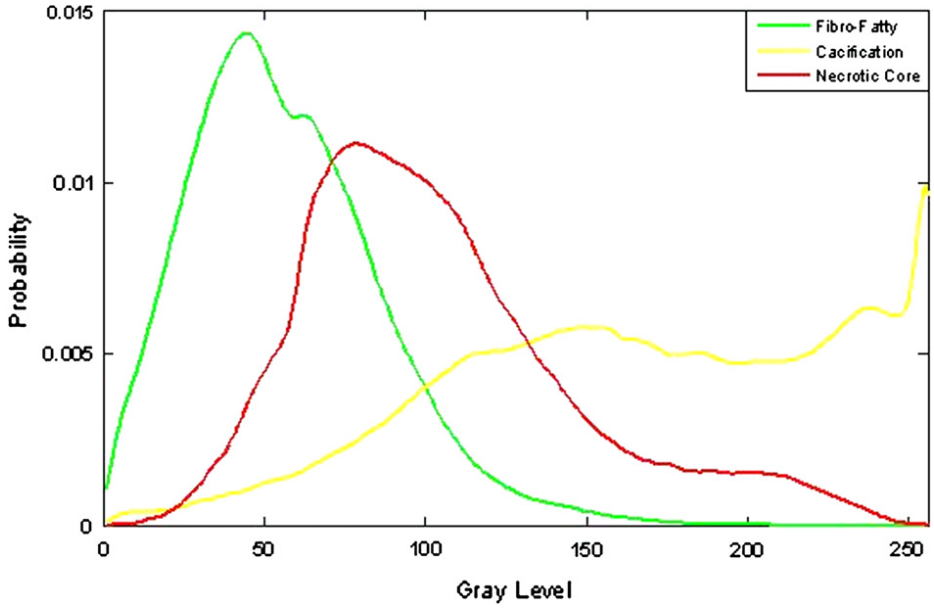

Fig. 5. The histogram of pixels belonging to fibro-fatty (FF), calcification (CA) and necrotic core (NC) classes for 400 out of 500 IVUS images.

whereas the few pixels with value under 50 (*ThCA* (high) = 50) belong to this class.
- Pixels belonging to the NC are concentrated mostly between 30 to 200 gray-levels (*ThNC*(low) = 30) and (*ThNC*(high) = 200).

Therefore, based on these additional thresholds, the system will decide on whether to change the decision of SVM classifier or not. To summarize the postprocessing section, the label assigned to a sample pixel and its gray-level are considered in the postprocessing step. Then, the pixel final labels are decided by this step. For instance, suppose the classification section assigns a pixel to the FF class and the gray-level of that pixel is above 150. In this case, based on *ThFF*, the current label declines and whether the gray-level is above *ThCA*(low) = 200 or not is determined. It will be assigned to the CA or NC class, respectively.

Statistical analysis

To assess the performance of our plaque characterization technique, the sensitivity, specificity and accuracy parameters were calculated for the different conditions (*i.e*. with or without shadow detection and with or without postprocessing) and for different feature extraction methods (*i.e*. LBP and the extended run-length methods). To calculate the agreement of our method with VH, Cohen's κ (Cohen 1960) and p value are used as statistical measures of concordance. A κ value of 0.61 to 0.80 indicates good agreement and 0.81 to 1.0 indicates excellent agreement (Fleiss 1981). Furthermore, the confidence interval (CI) is the other statistical measure employed to evaluate the reliability of our results.

Cross validation classification (CVC)

A five-fold cross validation approach is considered for validating our proposed algorithms. In this validation scheme, first, feature vectors extracted from all images of the data set are joined with each other to form a feature matrix. Then, this matrix is shuffled so that feature vectors of different classes are distributed randomly. After shuffling, this matrix is divided into five equal parts. In each validation step, four parts are considered as training data set used to train the classifier. The trained classifier is then tested with the remaining part. This procedure is repeated five times, each time with a new part as test data. Finally, the averages of the results derived from all steps are reported as the total result of classifier. These results are known to be more reliable than the other validation methods when sufficient number data is available (Duda et al., 2001).

Practical implementation

In this study, the proposed methods for border detection and plaque characterization were implemented in Matlab. These Matlab programs with a graphic user interface (GUI) were compiled by C++ compiler in Microsoft Visual Studio 2005. This GUI is designed as an effective image processing tool for IBH that enables cardiologists with complete IVUS image processing from border detection to plaque characterization.

RESULTS

The data was acquired from 10 patients, including about 2263 gray-scale IVUS images and their corresponding VH images. A total number of 500 frames from 12 vessels [six left anterior descending (LAD), three right coronary artery (RCA), three left circumflex (LCX)] of 10 patients were available for VH analysis and comparing with IBH. In the VH analysis, the total average amount of fibrous/fibro-fatty, dense calcium and necrotic core were (1,505,907 pixels) 37647 mm^2, (388,073 pixels) 9701 mm^2 and (516,711 pixels) 12917 mm^2, respectively. The relative average amounts per cross-section were 63%, 16% and 21%. Considering the shadow region detection procedure, 8% of plaque area pixels belong to the shadow region. The characterized IVUS images were validated by their corresponding VH images. A five-fold cross validation classification (CVC) scheme was used to evaluate the algorithm performance. To demonstrate the influence of applying the preprocessing step

Table 2. Results of pixel-wise plaque characterization of vessels' plaque area using the LBP method as feature extraction and SVM classifier

Histogram-based post-processing	Shadow detection	CA		FF		NC		Overall accuracy
		Sen.	Spec.	Sen.	Spec.	Sen.	Spec.	
No	No	68% ± 6.6	96% ± 3.2	97% ± 3	42% ± 6.6	06% ± 4.6	95% ± 3.2	66% ± 6.1
No	Yes	68% ± 6.6	94% ± 3.1	95% ± 3	45% ± 6.6	13% ± 4.5	94% ± 3.2	69% ± 6
Yes	No	69% ± 6.4	96% ± 3.2	70% ± 5.8	61% ± 5.2	39% ± 6.1	79% ± 5.7	67% ± 6.1
Yes	Yes	69% ± 6.4	95% ± 3.1	75% ± 5.8	81% ± 5.2	42% ± 6.6	76% ± 5.7	69% ± 5.8

The cases of including the pre- and postprocessing steps or not is distinguished using "Yes" and "No" signs in the two left columns. The parameter ± confidence interval is shown for the sensitivity (Sen.), specificity (Spec), and accuracy parameters.

FF = fibro-fatty; NC = necrotic core; CA = calcification; LBP = local binary pattern; SVM = support vector machine.

Table 3. Results of pixel-wise and region based plaque characterization of vessels' plaque area using the run-length method as feature extraction and SVM classifier

Histogram-based postprocessing	Shadow detection	DC		FF		NC		Overall accuracy
		Sen.	Spec.	Sen.	Spec.	Sen.	Spec.	
No	No	79% ± 6.5	93% ± 3.8	87% ± 5.1	38% = 5.	07% ± 3.3	97% ± 2.5	72% ± 6.3
No	Yes	79% ± 6.5	93% ± 3.7	96% ± 3	55% ± 6.6	12% ± 4.2	96% ± 2.7	74% ± 5.8
Yes	No	80% ± 6.5	93% ± 3.7	73% ± 6	64% ± 6.5	43% ± 6.6	80% ± 5.3	74% ± 6.4
Yes (pixel based)	Yes (pixel based)	79% ± 6.5	85% ± 3.6	81% ± 5.6	90% ± 5.3	52% ± 6.6	82% ± 5.5	75% ± 6.1
Yes (region based: 9×9 pixels)	Yes (region based: 9×9 pixels)	71% ± 4	97% ± 1	88% ± 1	87% ± 1	57% ± 4	88% ± 1	85% ± 3

The cases of in chiding the pre- and postprocessing steps or not is distinguished using "Yes" and "No" signs in the two left columns. The parameter ± confidence interval is shown for the sensitivity (Sen.), specificity (Spec) and accuracy parameters.
FF = fibro-fatty; NC = necrotic core; CA = calcification; SVM = support vector machine.

(*i.e.*, detecting the shadow region and assigning it to the fourth class) and the postprocessing derived from the histogram analysis, Table 2 and Table 3 illustrate the comparative results of the two different feature extraction methods considering different conditions. Considering the VH as our validating standard, we computed the κ to be 0.61 for the extended run-length (for both pixel based and region-based validations). Table 4 illustrates the p value for the case of applying both shadow detection preprocessing and histogram-based postprocessing and using the extended run-length method as a technique for feature extraction. Figure 6 shows the influence of shadow region detection preprocessing on the final reconstructed IBH image. Figure 7 illustrates the influence of postprocessing derived from histogram analysis on the final reconstructed IBH image. Finally, Figure 8 shows the final reconstructed IBH images for two feature extraction methods.

Moreover, in the last row of Table 3, the reconstructed images generated by using extended RL features are validated with their corresponding VH images using a region-based approach. It means that instead of comparing the result and its corresponding label pixel by pixel, the validation step is completed done by comparing regions of windows that contains more than one pixel. For example, the size of validation regions in (Nair et al. 2007) is 1/3 mm × 1/3 mm (*i.e.* approximately a window size of 13 × 13 pixels). To handle this, we define a validation window of size n × n pixels, where n can vary from one pixel-based validation to 13. The label of a validation window is selected by looking at labels of its constituent pixels. In fact, it is assigned to a plaque component that is the majority.

DISCUSSION

In this article, a complete algorithm for the IVUS image analysis including border detection to plaque characterization with more emphasis in the latter part is presented. This comprehensive image-based algorithm provides cardiologists with not only the vessel's intima and media-adventitia borders but also with a color-coded IBH image in which the location and distribution of different plaque components of atherosclerotic plaques are illustrated.

Perhaps, one of the important advantages of our proposed algorithm is to increase the longitudinal resolution of plaque composition analysis. The present VH-derived plaque composition analysis provides only ECG triggered images. As mentioned above, in an imaging procedure with the rate of 30 frames/s, only one IVUS frame out of approximately 30 IVUS frames is considered to generate the color-coded VH image. It can be concluded that in a typical VH imaging procedure about 96% of data will be discarded. Considering only VH images, the variations in area of different plaque components and their distribution in 1 mm intervals between VH images is missed. Tracking these small changes may reveal more precise information to physicians about plaque composition in the section of the vessel under consideration. To clarify this statement, the mentioned variations are highlighted in the charts shown in Figure 9. These charts illustrate the number of each plaque component in an IVUS frame. Here, 10 additional IVUS images between a pair of sequential VHs are characterized with the use of our proposed method. Increasing the

Table 4. The p value shows differences of the case of applying both shadow detection preprocessing and postprocessing and using the run-length method as a technique for feature extraction against the run-length method without preprocessing and histogram-based postprocessing

Parameter	Sen. CA	Sen. FF	Sen. NC	Spec. DC	Spec. FF	Spec. NC	Accuracy
p value	0.02781	0.01827	0.00497	0.02607	0.00695	0.01397	0.02345

(Sen.) = sensitivity; (Spec.) = specificity; FF = fibro-fatty; NC = necrotic core; CA = calcification.

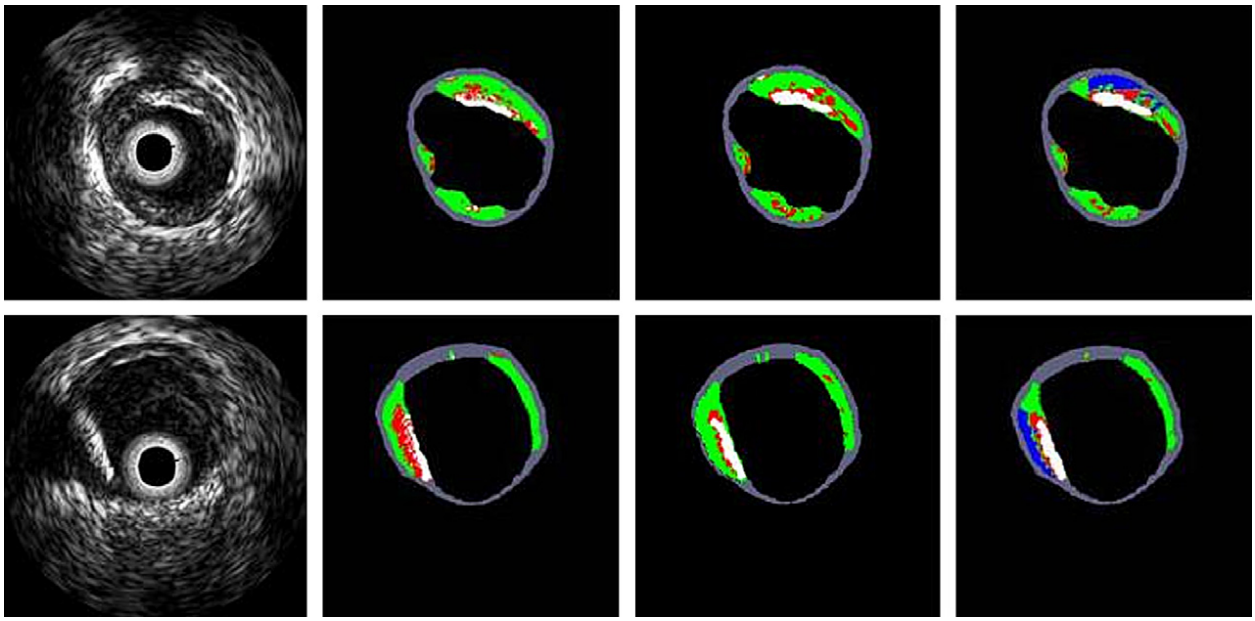

Fig. 6. The influence of applying the shadow detection section in the final constructed color-coded image based histology (IBH) images. The images are from left to right: a typical intravascular ultrasound (IVUS) image, its corresponding virtual histology (VH) image, IBH images without shadow section and with shadow detection section using the extended run-length feature extraction method. Note that the illustrated IBH images are after applying the histogram-based postprocessing technique. (The fibro-fatty (FF), NC and CA plaques are shown in green, red and white, respectively. The shadow region is in blue).

longitudinal resolution becomes more interesting when one tends to have a 3-dimensional view of both the vessel and the distribution of different plaque types in the plaque area.

As shown in Figure 2, our proposed algorithm contains different sections including plaque area detection, shadow region detection as a preprocessing, textural feature extraction, classification by SVM and

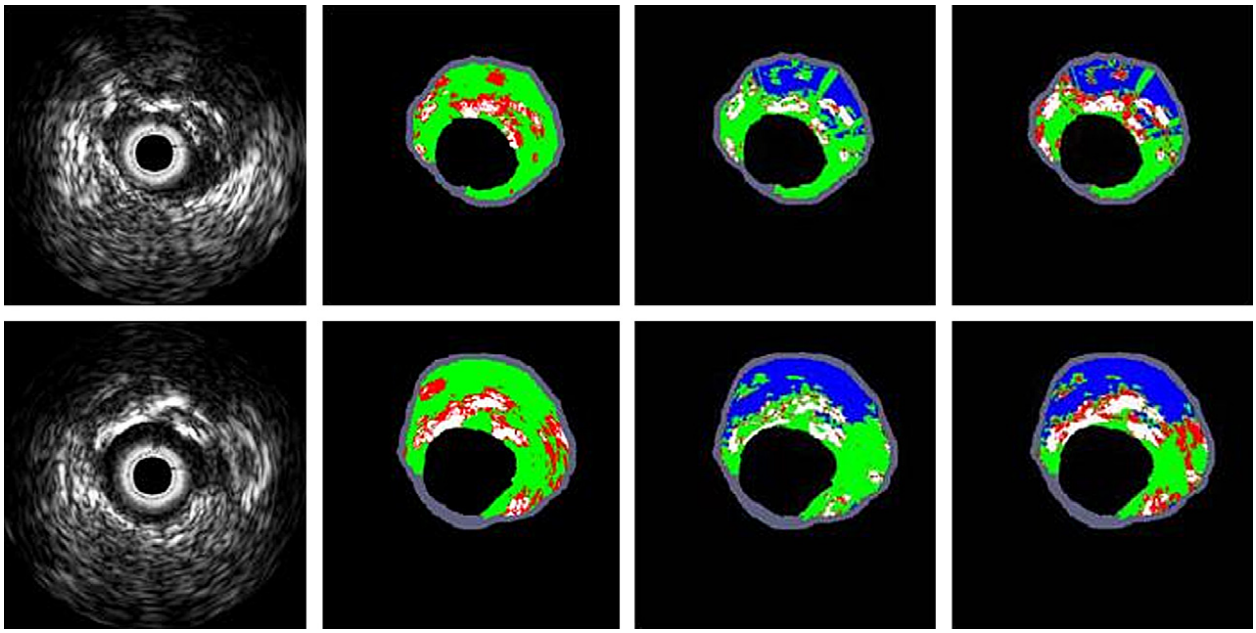

Fig. 7. The influence of applying the histogram-based postprocessing section in the final constructed color-coded image based histology (IBH) images. The images are from left to right: a typical intravascular ultrasound (IVUS) image, its corresponding virtual histology (VH) image, IBH images before applying the histogram-based postprocessing and after that using the LBP feature extraction method. Note that the illustrated IVUS-IBH images are after applying the shadow detection technique. The fibro-fatty (FF), necrotic core (NC) and calcification (CA) plaques are shown in green, red and white, respectively. The shadow region is in blue).

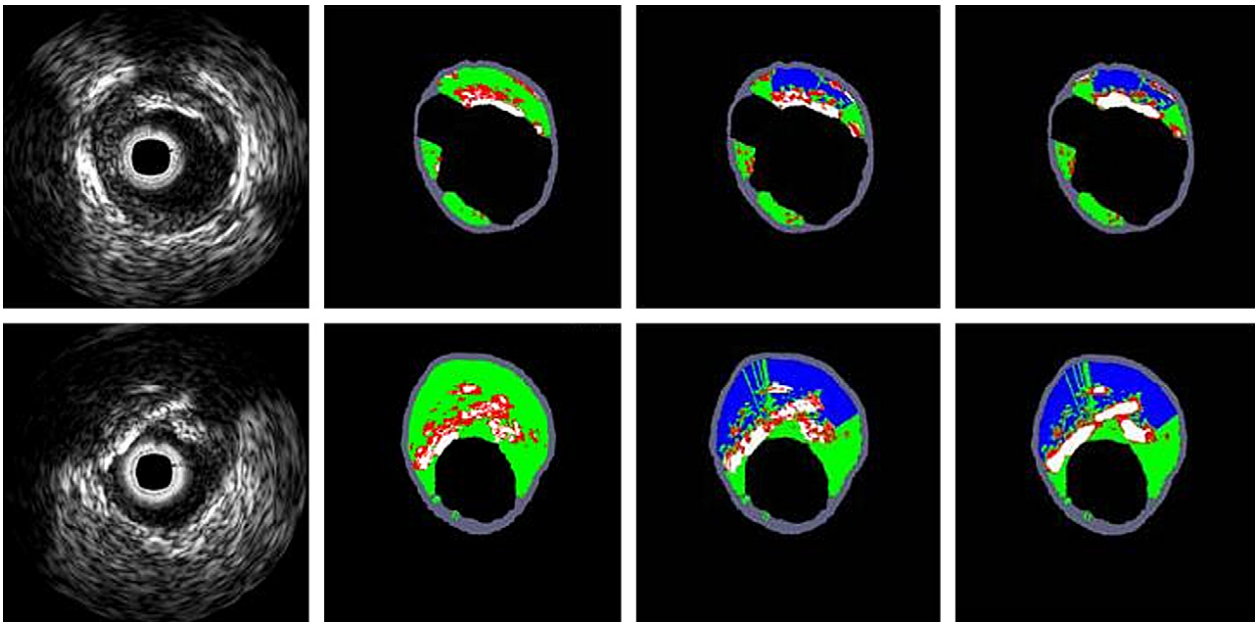

Fig. 8. The final constructed color-coded intravascular ultrasound-image based histology (IVUS-IBH) images using the proposed algorithm. From left to right: An IVUS image, its related virtual histology (VH) image and its IVUS-IBH images using the extended run-length and the LBP feature extraction methods.

postprocessing based on the data derived from the histogram analysis. We will discuss each part separately to present a clear view of the achievements in each part.

The differences in the results of the Tables 2 and 3 and those illustrated in Figure 7 show the influence of adding the shadow region detection as a preprocessing section. One of the obvious advantages to add the shadow region detection is to help algorithm to improve the detection of all three kinds of atherosclerosis plaque components. Moreover, this technique provides us with a more general algorithm that can be more reliable when studying patients with calcified plaques in which, a lateral shadow region exists behind the calcified area. Out of the total number of 191,582 pixels contained in the shadow region, 63%, 36% and about 1% were characterized into FF, NC and CA plaques by the VH algorithm, respectively. Therefore, Tables 2 and 3 show that in addition to improving the distinction of three plaque components, the shadow detection procedure has a direct influence on the detection of FF and NC. Differences of relative amounts of CA and NC after and before shadow detection were calculated to be 5% and 4%, respectively. One should note that the IVUS-IBH images in the third and fourth column of Figure 7 show small islands of green within the blue shadow regions. These islands normally are not expected, as the RF signal is attenuated due to the shadowing caused by the calcium. However, multiple reflections between the catheter and the calcium, known as reverberations, can lead to appearance of these islands.

By comparing the results of the Table 2 and Table 3, it can be concluded that the extended run-length feature extraction method outperforms the LBP in classifying all plaque components. However, as illustrated in Figure 8, it is quite clear that the color-coded image reconstructed with the use of LBP feature extraction method is more detailed. This may be caused by the multiresolution characteristic of this method. Perhaps, one future direction is to combine these two feature extraction methods to benefit from their both detailed and accurate results.

The computation times of the feature extraction methods are as follows: for a typical frame, *i.e.*, the plaque area containing around 5000 pixels out of the total 160,000 IVUS image pixels, the extended run-length method took approximately 7 to 20 s to extract the features whereas the LBP took 2 to 5 min. Thus, in terms of time efficiency, the extended run-length method further outperforms the LBP method. However, a more optimized implementation in C++ will further speed up the algorithms as expected. The influence of the postprocessing block after classification is highlighted in the differences in the sensitivity and specificity of the algorithm in characterizing NC and FF plaques, respectively. The extensive textural similarities between the NC regions and other plaque components defined by VH leads to preventing the classification part of the algorithm from identifying it; however, by studying the distribution of plaques' intensities in the data set, it is concluded that in addition to textural features, there exists some rules for distinguishing the plaques in it (Fig. 5).

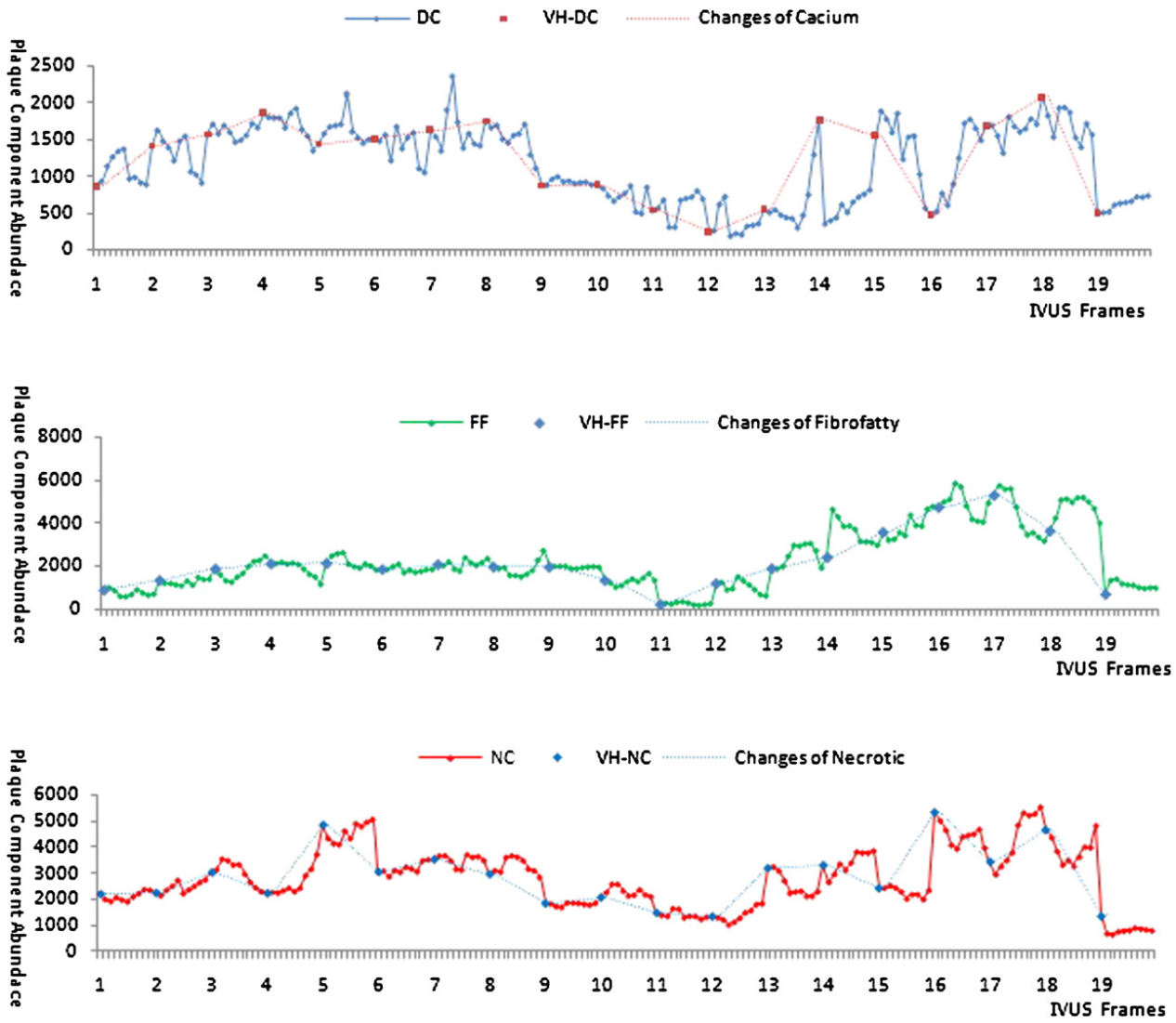

Fig. 9. Illustration of (a) calcium, (b) fibro-fatty and (c) necrotic core changes between virtual histology (VH) slides.

The results of region-based validation approach (refer to last row of Table 3) show that the result of the algorithm is sensitive to the approach of validation. Since in most similar studies region-based approach is considered for validation and more specifically our labels are provided by VH, which is also validated by this approach, superiority of this validation approach to the pixel-based one was predictable. We validated our reconstructed images with their corresponding VH images with different size of validation window. Based on the experiments, obtained results are sensitive to the size of validation window and the maximum accuracy occurs when n is set to nine. Since nine is also the size of sweeping window in feature extraction step, it encourages the idea that the size of sweeping window might have influence on the size of validation window. The κ number = 0.61(for both pixel based and region based validation) clearly represents that our classification results are in good agreement with VH after detecting and removing shadow regions. Moreover, the low values of CI and p value show the reliability and consistency of these results obtained for this data-set. The p values indicated in Table 4 answer the following question: If our method's performance is the same as before with applying shadow detection and postprocessing, what is the probability of observing the current result? From a statistical point of view, the observed difference in our results compared to the results of our methods before detecting shadow and applying postprocessing is not accidental.

An interesting point to be mentioned here is that the presented results suggest that the texture based algorithm based on IVUS gray-scale images produces similar images and has a modest co-relation to VH-IVUS, suggesting that most of the information in VH-IVUS tissue

characterization comes from the intensity of the ultrasound signal and less-so on the underlying radio-frequency data.

In this study, all methods' sensitivity to detect the NC was low (maximum value is 57%). The fact that detection of NC by studying the IVUS images is not a straightforward procedure has also been previously discussed in (Gonzalo et al., 2008; Nasu et al., 2006). This phenomenon was caused by similarities between NC and CA in gray-level IVUS images. This fact supports the previous studies, which have shown that plaque areas adjacent to dense calcium are frequently coded as necrotic tissue in VH images (Sales et al., 2008). By considering selected cross-sections that contained plaque areas with a homogeneous tissue composition as reported in (Gonzalo et al., 2008), the accuracy results can be increased significantly.

Although the sensitivity of detecting the calcified region was 79%, the algorithm performance to detect the focal calcified region in the images was more than 85%, which is another important point about these results. It derives from the fact that in the VH method, the variation of pixels intensities assigned to the calcium class is very high (from 0 to 256) as can be observed in Figure 5. However, since identifying focal calcified regions are more important than speckled calcification in the plaque area, our proposed algorithm shows increased reliability (Virmani et al., 2003).

Limitations

In general, there are some differences between the image and signal processing techniques. In signal processing methods, the frequency information of RF signal is used along with its amplitude, whereas in image processing techniques, decisions are made from the variations in the distribution of gray-levels produced solely from the amplitude information of the RF signal. Hence, there is a possible loss of information in image processing techniques. On the other hand, an advantage of the proposed algorithm is that it can reliably classify tissues regardless of the variations in the power spectrum of the transducer while inconsistency among the spectrum-derived features within the transducer's bandwidth still remain a major challenge (Katouzian et al., 2008a, 2008b). However, this does not assert that our proposed method is robust to the changes in the transducer's center frequency since the texture of tissue in IVUS images is very different with different frequencies, different transducer bandwidths and different transducer geometries. One of the main limitations of our study is employing the VH images for training our classifier. Although VH imaging has an acceptable correlation with histology (Nasu et al., 2006), is used clinically (König and Klauss 2007) and has approved performance in many studies (Gonzalo et al., 2008; Nair et al., 2002, 2007), even a subtle error of VH can influence the entire procedure. Therefore, VH-IVUS can be considered as a basis for comparing similar plaque component characterization algorithm via IVUS images or signals but it should not be considered definitive. Therefore, we hope to overcome this limitation in our future study by employing other types of the constructed images, applying other techniques such as the one introduced in (Katouzian et al., 2008b) and using the real histology images as our gold standard.

As mentioned above, by combining the fibrous and the fibro-lipid classes, the number of classes was reduced from four to three. The similarities of these two classes in VH images were also reported in (Katouzian et al., 2008b). They mentioned that these kinds of similarities come from normalizing the spectrum of IVUS backscattered signal with respect to the catheter and also not extracting the most discriminative features from the spectrum of IVUS backscattered signal in the VH method. The next challenge is to further classify the fibrous and fibro-lipid regions. As our algorithm's parameters are achieved from the training process by the VH images, we should note that one should consider the variation of VH images by changing the IVUS catheter. Therefore, as part of our future work, the number of case studies with different IVUS transducers will be increased. Furthermore, identifying thrombus and stent struts are possible future extensions of this study.

CONCLUSION

In this article, we proposed an efficient algorithm for automatic IVUS image border detection and particularly for plaque characterization. Based on this study's findings, the extended run-length feature extraction method seems to be superior to the LBP method in terms of both time efficiency and classification accuracy. Moreover, adding a shadow detection block as a preprocessing step and a threshold based postprocessing step derived from the histogram analysis of VH data-set, has positively affected the whole algorithm performance. *In vivo* validation procedures were used where the results showed the efficiency of the proposed algorithm for vessel plaque characterization via IVUS images. A graphic user interface (GUI) is designed as an effective image processing tool that enables cardiologists with complete IVUS image analysis from the border detection to plaque characterization.

Acknowledgments—The authors would like to thank Sara Avansari for helping them with the simulation. The authors gratefully acknowledge the anonymous referees for several suggestions and references.

REFERENCES

Böse D, von Birgelen C, Erbel R. Intravascular ultrasound for the evaluation of therapies targeting coronary atherosclerosis. J Am Coll Cardiol 2007;49:925–932.

Bruining N, Verheye S, Knaapen M, Somers P, Roelandt JR, Regar E, Heller I, de Winter S, Ligthart J, Van Langenhove G, de Feijter PJ, Serruys PW, Hamers R. Three- dimensional and quantitative analysis of atherosclerotic plaque composition by automated differential echogenicity. Catheter Cardiovasc Intervent 70 doi:10.1002/ccd. 2131. 2007;70:968–978.

Burges C. Tutorial on support vector machines for pattern recognition. Data mining Knowledge Discov 1998;2:955–974.

Caballero K, Barajas J, Pujol O, Salvatella N, Radeva P. *In vivo* ivus tissue classification: A comparison between RF signal analysis and reconstructed images. CIARP06, LNCS 4225 2006;3:137–146.

Chang CC, Lin CJ. A library for support vector machines. Available at: http://www.csie.ntu.edu.tw/ cjlin/libsvm. Accessed 2001.

Cohen J. A coefficient of agreement for nominal scales. Educ Psychol Meas 1960;20:37–46.

Duda R, Hart P, Stork D. Pattern classification. 2nd ed. New York: Wiley; 2001. Chapter 9. p. 453–517.

Escalera S, Pujol O, Mauri J, Radeva P. Intravascular ultrasound tissue characterization with sub-class error-correcting output codes. J Signal Process Sys 2008.

Fleiss J. Methods for rates and proportions. 2nd ed. New York: John Wiley & Sons; 1981.

Frutkin A, Mehta S, McCrary J, Marso S. Limitations to the use of virtual histology- intravascular ultrasound to detect vulnerable plaque. Eur Heart J 2007;28:1783–1784.

Gonzalo N, Garcia-Garcia H, Ligthart J. Coronary plaque composition as assessed by gray-scale intravascular ultrasound and radiofrequency spectral data analysis. Int J Cardiovasc Imaging doi: 10.1007/ s10554-008-9324-2. 2008;24:811–818.

Haralick R, Shanmugam K, Dinstein I. Textural features of image classification. IEEE Trans Syst Man Cyber 1973;6:610–621.

Hiro T, Leung C, Guzman SD, Caiozzo V, Farvid A, Karimi H, Helfant R, Tobis J. Are soft echoes really soft? Intravascular ultrasound assessment of mechanical properties in human atherosclerotic tissue. American Heart J 1997;133:1–7.

Katouzian A, Baseri B, Konofagou E, Laine A. Texture-driven coronary artery plaque characterization using wavelet packet signatures. IEEE Int Symp Biomed Imaging From Nano to Macro (ISBI) 2008. p. 197–200.

Katouzian A, Sathyanarayana S, Baseri B, Konofagou E, Carlier S. Challenges in atherosclerotic plaque characterization with intravascular ultrasound (ivus): From data collection to classification. IEEE Trans Inform Technol Biomed 2008b;12:315–327.

Kawasaki M, Ito Y, Yokoyamaa H, Arai M, Takemura G, Hara A, Ichiki Y, Takatsu H, Minatoguchi S, Fujiwara H. Assessment of arterial medial characteristics in human carotid arteries using integrated backscatter ultrasound and its histological implications. Atherosclerosis 2005;180:145–154.

König A, Klauss V. Virtual histology. Heart 2007;30:977982.

König A, Margolis M, Virmani R, Holmes D, Klauss V. Technology insight: *In vivo* coronary plaque classification by intravascular ultrasonography radio-frequency analysis. Cardiovasc Med 2008;5: 219–229.

Mintz G, Nissen S, Anderson W. American College of cardiology clinical expert consensus document on standards for acquisition, measurement and reporting of intravascular ultrasound studies (ivus). A report of the american college of cardiology task force on clinical expert consensus documents. J Am Coll Cardiol 37. doi:10.1016/S0735-1097(01)01175-5. 2001;37:1478–1492.

Nair A, Kuban B, Tuzcu EP, Schoenhagen P, Nissen SE, Vince DG. Coronary plaque classification using intravascular ultrasound radiofrequency data analysis. Circulation 2002;106:2200–2206.

Nair A, Margolis MP, Kuban BD, Vince DG. Automated coronary plaque characterization with ivus backscatter *ex vivo* validation. Eur Intervent 2007;106:2200–2206.

Nasu K, Tsuchikane E, Katoh O, Vince DG, Virmani R, Surmely J, Murata A, Takeda Y, Ito T, Ehara M. Accuracy of *in vivo* coronary plaque morphology assessment. J Am Coll Cardiol 2006;47: 2405–2412.

Ojala T, Pietikainen M, Maenpaa T. Multiresolution gray-scale and rotation invariant texture classification with local binary patterns. IEEE Trans PAMI 2002;24:971–987.

Okubo M, Kawasaki M, Ishihara Y, Takeyama U, Kubota T, Yamaki T, Ojio S, Nishigaki K, Takemura G, Saio M, Takami T, Minatoguchi S, Fujiwara. H. Tissue characterization of coronary plaques: Comparison of integrated backscatter intravascular ultrasound with virtual histology intravascular ultrasound. Circ J 2008;72:1631–1639.

O'Malley SM, Carlier SG, Naghavi M, Kakadiaris IA. Image-based frame gating of ivus pullbacks: A surrogate for ecg. ICASSP 2007;I-433–I-436.

Sales F, Falcao J, Falcão BAA, Lemos PA, Furuie SS. Evidences of possible necrotic-core artifact around dense calcium in virtual histology images. Computers in Cardiology Conference 2008;35: 545–548.

Sangiorgi G, Clementi F, Cola C, Biondi-Zoccai G. Plaque vulnerability and related coronary event prediction by intravascular ultrasound with virtual histology: It's a long way to Tipperary? Catheter Cardiovasc Intervent 2007;70:203–210.

Sawada T, Shite J, Garcia-Garcia H, Takahiro Sawada, Shite J, *Garcia-Garcia M, Hector M, Shinke T, Watanabe S, Otake H, Matsumoto D, Tanino Y, Ogasawara D, Kawamori H, Kato H, Miyoshi N, Yokoyama M, Serruys PW, Hirata K. Feasibility of combined use of intravascular ultrasound radiofrequency data analysis and optical coherence tomography for detecting thin-cap fibro-atheroma. Eur Heart J 2008;29:1136–1146.

Taki A, Najafi Z, Roodaki A, Setarehdan SK, Zoroofi R, König A, Navab N. Automatic segmentation of calcified plaques and vessel borders in ivus images. Int J Comput Assist Radiol Surg (CARS) 2008;3:347–354.

Taki A, Roodaki A, Pauly O, Setarehdan SK, Unal G, Navab N. A new method for characterization of coronary plaque composition via ivus images. IEEE International Symposium on Biomedical Imaging: From Nano to Macro (ISBI 2009);787–790.

Tang X. Texture information in run-length matrices. IEEE Tran Image Process 1998;7:1602–1609.

Unal G, Bucher S, Carlier S, Slabaugh G. Shape-driven segmentation of arterial wall in intravascular ultrasound images. IEEE Trans Inform Technol Biomed 2008;12:335–347.

Vince D, Dixon K, Cothren R, Cornhill J. Comparison of texture analysis methods for the characterization of coronary plaques in intravascular ultrasound images. Comput Med Imaging Graph 2000;24:221–229.

Virmani R, Burke AP, Kolodgie FD, Farb A. Pathology of thin-cap fibroatheroma: A type of vulnerable plaque. J Intervent Cardiol 2003;16:267–272.